A semi-analytical solution of three-dimensional transient temperature field for a uniform plate subjected to Gaussian-distribution laser heat source

Xiaogui WANG[1], Yili XIAO[1], Ninghua GAO[2], Lihua LIANG[1], Congda LU[1], Haojie JIANG[*1]

[*1]College of Mechanical Engineering, Zhejiang University of Technology, Hangzhou 310023, China

[2]Department of Big Data Science, School of Science, Zhejiang University of Science and Technology, Hangzhou 310023, People's Republic of China

[*]Corresponding author; E-mail: haojjiang@zjut.edu.cn

Abstract: One three-dimensional transient temperature field model for a thin uniform plate caused by a moving laser heat source is described in present study. The heat source model with a power density in Gaussian-distribution form is considered when a finite-thin uniform plate is heated. By using the separate variable method (SVM) and the Newton Cotes method (NCM), a semi- analytical solution of three-dimensional heat conduction equation in the finite field is obtained. Numerical results show that the effect of laser heat source distribution, laser moving speed as well as aspect ratio of the thin uniform plate have great influence on the three-dimensional distribution of the temperature field.

Key words*: Three-dimensional temperature distribution; Gaussian-distribution heat source; Separate variable method; Newton Cotes method*

1. Introduction

Lasers were widely used [1-5] in various processing and manufacturing fields due to their features such as high efficiency, easy power adjustment and no force during processing. The temperature of the material was increased by the heat of the laser [6]. When the temperature rises to a certain degree, the material would break, melt and deform. Therefore, it is particularly important to perform temperature prediction and controlling during laser operations to avoid dangerous thermal stresses.

There were some problems in the practical application of laser assisted processing. For instance, determining the optimal process parameters of the laser [7-9], the interaction mechanism of the laser and the material (such as the absorptivity of the material to the laser [10-12], the penetration ability of the laser to the material [13,14], and the phase change of the laser to the material influences [15-18], etc.). Therefore, a large number of experimental studies were conducted. Experiments [19-23] were conducted to evaluate the potential of laser-assisted processing in the economic feasibility of manufacturing precision ceramic components. Comparing the surface damage of parts produced by laser-assisted processing with the damage of typical grinding parts [24], the results showed that the most significant advantages of laser-assisted processing could achieve higher material removal rate, more excellent workpiece surface quality and well reasonable tool wear levels. Accurately measuring the temperature field of a workpiece during laser processing was extremely difficult, and it often required many previous tests to set the suitable laser process [25] for certain materials, this would

require a lot of manpower, material and financial resources. Besides, human error in operation and the advancement of measuring instruments all affect the final experimental results.

With the rapid development of computer software and hardware technology, virtual manufacturing technology has caused an upsurge, and numerical simulation has gradually behaved its superiority [26]. In terms of numerical simulation, regarding the laser source as a concentrated heat source, Gutierrez and Araya [27] developed a numerical simulation of the temperature distribution generated by a moving laser beam for a finite field. Comparing with the analytical solution in the semi-infinite field [28], slightly higher temperatures were produced in the regions that close to the boundary. The two temperature profiles actually coincided at that far away from the border. By using finite element analysis software (ANSYS), Han et al. [29] simulated the temperature distribution of the laser welding of the 304 stainless steel plate dynamically. The calculation showed that the simulation results of the weld shape agreed well with the experimental results. Considering the effects of phase transition potential [30,31] as well as thermal, structural and plastic deformations, Yao and Chen [32] presented a three-dimensional finite element model for the calculation of transient thermal and residual stresses, besides, the numerical simulation of the thermal field and residual stress field during laser processing was studied. The numerical example verified that the current model was better than other models that had been proposed, but there also existed errors comparing with the experimental results. The finite element model was used to simulate the sintering process of Ni-Gr coatings on AISI 4140 steel [33] numerically, and the distribution and evolution of its temperature field was also studied, single-track experiments were performed with the same laser sintering parameters as the simulations, the results showed the correctness of the simulation. Li et al. [34] developed a three-dimensional thermo-mechanical coupling model to simulate a multi-track, multilayered selective laser melting process by using the finite element method. The numerical solution was generally a solution obtained using a finite element method, a numerical approximation method, an interpolation method and so on. However, the calculated values corresponding to any independent variables as well as the value of the independent variables subject to certain restrictions of the numerical method could not be obtained. Thus, the semi-analytical solutions were often introduced to solve these problems effectively.

In terms of theoretical calculations, Elsen et al. [35] studied the analysis and numerical solution of the heat conduction equation for any type of local moving heat source for laser shock processing. Cheng and Lin [36] established an analytical model that describing a three-dimensional temperature field that using a Gaussian heat source moving at a constant velocity, and the computation time of analytical solution cost less when comparing with the finite element method and the finite difference method. Considering the cooling effect caused by free or forced convection in the ambient gas, Brockman et al. [37] calculated a two-dimensional temperature field in a sheet moving slice heated with a laser beam, and a two-dimensional integral Fourier transform on the space coordinates was used by them to solve the problem as well as the analytical solution of the problem in Fourier space was obtained. Jiang and Dai [38] solved the three-dimensional steady heat conduction problem of a double-layer plate by using the Poisson method and the layer wise approach, where the double-layer structure including a coating layer and FGM layer, in addition, the separation of variables method and the layer wise approach were used to solve the three-dimensional transient thermal conduction problem. Taking into consideration the solid-liquid-vapor phase-change process [39] and the simply supported conditions [40] respectively, Jiang et al. solved the three-dimensional transient temperature

field of a high strength and low alloy rectangular steel plate under laser shock processing by the separate variable method. Considering the trajectory of the source was approximately a straight line as well as surface heat source model was regarded as a Gaussian-distribution of power density, Winczek et al. [41] described a three-dimensional transient temperature field in a semi-infinite body caused by a moving laser heat source with any trajectory. Chen et al. [42] gave a short review of the harmonic general solutions for uncoupled elasticity of transversely isotropic materials with thermal and other effects.

Most of analytical solutions encountered in the literatures were based on an infinite domain, semi-infinity domain as well as quasi-steady state at a constant speed for heat source. Few works referred to complete semi-analytical solutions for three-dimensional transient heat conduction, and only the temperature evolution caused by a uniform heat source was described. Present paper focus on the Gaussian-distribution of laser heat source for temperature model in the uniform plate firstly. Then, the result of paper is compared with that of numerical simulation and shows the accuracy of the present method. Finally, the effects of heat source distribution, laser moving speed and the aspect ratio of length to width for the uniform plate on the distribution of the temperature field is analyzed.

2. Mathematical modeling

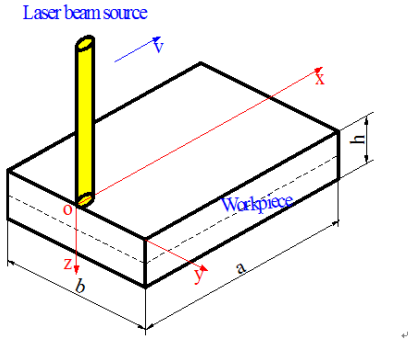

Fig.1. Schematic of the laser processing on a uniform Si_3N_4 plate

Fig.1 is a Si_3N_4 plate (whose dimensions in x, y and z directions are a, b and h, respectively) subjected to moving laser beam source with uniform velocity v along the x direction. The heat from laser source penetrates into the plate and generates a continuous heat flux q going into the plate with the passage of time t, thus the heat conduction model could be regarded as under the transient thermal environment.

The following assumptions are also considered in the present model [43]:

(i) The investigated Si_3N_4 plate is uniform and isotropic.

(ii) The physical properties such as thermal conductivity λ, density ρ and specific heat c of the structure are all constants.

(iii) Temperature jump or phase change does not occur in the temperature field for the plate.

With the above assumptions and considering three-dimensional heat conduction process, the transient heat conduction equation based on the energy conservation law can be written as follows:

$$\rho \times c \times \frac{\partial \Delta T}{\partial t} = \lambda_x \frac{\partial^2 \Delta T}{\partial x^2} + \lambda_y \frac{\partial^2 \Delta T}{\partial y^2} + \lambda_z \frac{\partial^2 \Delta T}{\partial z^2} + q'''(x, y, z, t) \tag{1}$$

where $\lambda_i (i = x, y, z)$ are thermal conductivities along x, y and z directions, respectively. $\Delta T = T - T_0$ represents temperature variation for the uniform plate relative to surrounding environment temperature, $q'''(x, y, z, t)$ is the volumetric source term of heat generation.

2.1. Three-dimensional heat source modeling

The heat source term $q'''(x, y, z, t)$ is considered as a laser beam of temporal continuous wave and spatially modeled as a Gaussian-distribution. Fig.2 shows the transversal mode in a laser spot.

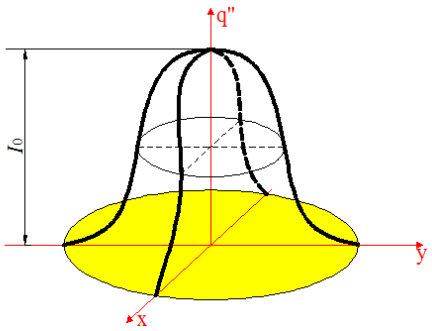

Fig.2. Transversal mode in a laser spot

The Gaussian heat flux distribution q'' takes the following exponent form:

$$q'' = \begin{cases} I_0 \times e^{\frac{-k\left(x^2+y^2\right)}{r^2}} & vt - r < x < vt + r, -\sqrt{r^2 - \left(x - vt\right)^2} < y < \sqrt{r^2 - \left(x - vt\right)^2}, and \quad z = 0 \\ 0 & otherwise \end{cases} \tag{2}$$

where I_0 is the intensity at the center of the spot, k is a constant (in general, a value of 2 is used for a Gaussian model), r is the laser spot radius, and with following form

$$r = \sqrt{\frac{s}{\pi}} \tag{3}$$

in which s is the laser spot area, besides heat flow absorbed by the workpiece q can be obtained by following expression:

$$\int_{-r}^{r} \int_{-\sqrt{r^2-x^2}}^{\sqrt{r^2-x^2}} I_0 \times e^{\frac{-k\left(x^2+y^2\right)}{r^2}} dydx = q \tag{4}$$

The relation between volumetric heat generation q''' and Gaussian-distribution heat flux q'' is defined as follows:

$$q''' = q'' \times \delta(z) \tag{5}$$

where $\delta(z)$ is the Dirac delta function.

2.2. Initial and boundary conditions

Boundary conditions at the six faces of the parallelepiped domain and an initial condition have to be specified. The initial condition of the temperature variation ΔT for the Si_3N_4 plate is as follows when the time equals to zero

$$\Delta T(x, y, z, 0) = 0 \tag{6}$$

Insulated conditions were imposed at $x = 0$ surface, i.e. with

$$\Delta T(0, y, z, t) = 0 \tag{7}$$

Meanwhile, Dirichlet temperature conditions were considered at $x = a$, $y = b/2$, $y = -b/2$ and $z = h$ surfaces. The main reason of selecting Dirichlet conditions at above-mentioned surfaces can be seen

in reference [43]. Besides, the top surface $z=0$ is considered to be adiabatic except for the heating area which powered by the moving laser beam.

In order to solve the three-dimensional transient temperature filed subjected to Gaussian-distribution heat flux, the temperature field $\Delta T(x,y,z,t)$ in Eq.(1) can be expressed by using the separate variable method (SVM).

$$\Delta T(x,y,z,t)=\sum_{o}\sum_{p}\sum_{q}\Theta(o,p,q,t)\times X(o,x)\times Y(p,y)\times Z(q,z) \tag{8}$$

According to the initial and boundary conditions (i.e. Eq.(6) and Eq.(7), respectively), the eigenfunctions $X(o,x)$, $Y(p,y)$ and $Z(q,z)$ which satisfied above-mentioned boundary conditions have the following forms, respectively:

$$X(o,x)=\cos[\alpha(o)\times x] \tag{9a}$$

$$Y(p,y)=\cos[\beta(p)\times y] \tag{9b}$$

$$Z(q,z)=\cos[\gamma(q)\times z] \tag{9c}$$

where the eigenvalues $\alpha(o)$, $\beta(p)$ and $\gamma(q)$ are, respectively

$$\alpha(o)=\frac{2\times o+1}{2a}\pi,\quad o=0,1,\cdots n \tag{10a}$$

$$\beta(p)=\frac{2\times p+1}{b}\pi,\quad p=0,1,\cdots n \tag{10b}$$

$$\gamma(q)=\frac{2\times q+1}{2h}\pi,\quad q=0,1,\cdots n \tag{10c}$$

And the non-homogeneous term q''' can be expanded in a linear combination of the eigenfunctions

$$q'''(x,y,z,t)=\sum_{o}\sum_{p}\sum_{q}\varphi(o,p,q,t)\times X(o,x)\times Y(p,y)\times Z(q,z) \tag{11}$$

By utilizing the orthogonality of eigenfunctions $X(o,x)$, $Y(p,y)$ and $Z(q,z)$, and multiplying them side-by-side for Eq. (11) as well as integrating over the whole dimensional domain, then Eq.(11) yields:

$$\begin{aligned}&\int_0^a\int_{\frac{-b}{2}}^{\frac{b}{2}}\int_0^h q'''(x,y,z,t)\times X(o,x)\times Y(p,y)\times Z(q,z)dxdydz\\&=\varphi(o,p,q,t)\times\int_0^a X^2(o,x)dx\int_{\frac{-b}{2}}^{\frac{b}{2}}Y^2(p,y)dy\int_0^h Z^2(q,z)dz\\&=\varphi(o,p,q,t)\times\frac{abh}{8}\end{aligned} \tag{12}$$

Substituting Eq.(2) and Eq.(5) into Eq.(12) and integrating it into the entire field, following equation can also be obtained.

$$\begin{aligned}&\int_0^a\int_{\frac{-b}{2}}^{\frac{b}{2}}\int_0^h I_0\times e^{\frac{-k\left(x^2+y^2\right)}{r^2}}\times X(o,x)\times Y(p,y)\times Z(q,z)\times\delta(z)dzdydx\\&=\int_{vt-r}^{vt+r}\int_{-\sqrt{r^2-(x-vt)^2}}^{\sqrt{r^2-(x-vt)^2}}I_0\times e^{\frac{-k\left((x-vt)^2+y^2\right)}{r^2}}\times\cos[\alpha(o)\times x]\times\cos[\beta(p)\times y]dxdy\\&=\varphi(o,p,q,t)\times\frac{abh}{8}\end{aligned} \tag{13}$$

3. Numeral calculations

It is so hard to solve the above Eq.(13) through direct integration, the Newton Cotes method (NCM) is considered on left side of Eq.(13), the NCW has following unified expression form:

$$C_m(f)=\sum_{i=0}^{m-1}\frac{l}{90}\times[7f(x_i)+32f(x_{i+1/4})+12f(x_{i+1/2})+32f(x_{i+3/4})+7f(x_{i+1})] \quad (14)$$

where C represents the abbreviation of NCM, subscript m denotes the number of divided segments, f denotes the function to be integrated, l is the length of each segment.

And the following equation should be satisfied for a given minimum accuracy ε:

$$\left|I(f)-C_{2m}(f)\right|\approx\frac{1}{63}\left|C_{2m}(f)-C_m(f)\right|\le\varepsilon \quad (15)$$

in which $I(f)$ represents the exact value of the quadrature function *f*. In this paper, the value of m is taken as 8 in this work, which not only satisfies certain accuracy requirements, but also saves the calculation time.

Finally, the expression of $\phi(o,p,q,t)$ can be obtained according to Eqs.(13) and (14).

Substituting the $\phi(o,p,q,t)$ into Eq.(11) and inserting it into Eq.(1) together with Eq.(8), then an ordinary differential equation for $\Theta(o,p,q,t)$ can be obtained:

$$\frac{1}{\alpha}\times\frac{d\Theta(o,p,q,t)}{dt}=-\frac{\omega(o,p,q)}{\alpha}\times\Theta(o,p,q,t)+\frac{\varphi(o,p,q,t)}{\lambda} \quad (16)$$

where

$$\alpha=\frac{1}{\rho c},\ \omega(o,p,q)=\{[\alpha(o)]^2+[\beta(p)]^2+[\gamma(q)]^2\}\times\alpha \quad (17)$$

And defining $\Omega(o,p,q,t)=\frac{a}{\lambda}\times\varphi(o,p,q,t)$, then Eq.(16) yields:

$$\frac{d\Theta(o,p,q,t)}{dt}+\omega(o,p,q)\times\Theta(o,p,q,t)=\Omega(o,p,q,t) \quad (18)$$

With the initial condition Eq.(6), there with $\Delta T=0$ when $t=0$. And the corresponding $X(o,x)$, $Y(p,y)$ and $Z(q,z)$ values are not always 0 for any x, y or z, hence the following equation can be finally obtained:

$$\Theta(o,p,q,0)=0 \quad (19)$$

The solution of $\Theta(o,p,q,t)$ can be obtained according to simultaneous equations (18) and (19). Then substituting the expression of $\Theta(o,p,q,t)$ into Eq.(8), the transient temperature field can be finally obtained.

4. Results and discussion

Tab.1

Thermophysical properties of silicon nitride (Si_3N_4)

Melting point $(°C)$	Density (kg/m^3)	Specific heat $(J/kg°C)$ @ 1000 °C	Thermal conductivity $(W/m°C)$ @ 1000 °C	Thermal diffusivity (m^2/s) @ 1000 °C
1900	2400	1278.96	5.91	1.9×10^{-6}

The semi-analytical solution is used for the laser heating process of the uniform Si_3N_4 plate, whose thermophysical properties [43-45] are summarized in Tab.1. The area of the laser circular spot $1\times10^{-6}\,m^2$

and the laser net power 50W are considered in present work. From the established Cartesian coordinate system (Fig.1), the temperature distribution on the workpiece is symmetrical about the X axis, hence considering half of the workpiece is enough. And referring to [43], it is determined that the 150 feature value is taken in each direction.

Example 1. The dimensions of the workpiece along the X, Y, and Z directions are 0.04m, 0.02m and 0.00625m, respectively. The laser moving speed 0.1m/s is considered, besides the k value of Gaussian heat source is selected as 3. When the laser moves to 0.25a at x direction, the temperature distribution along the x direction of workpiece is showed in Fig.3.

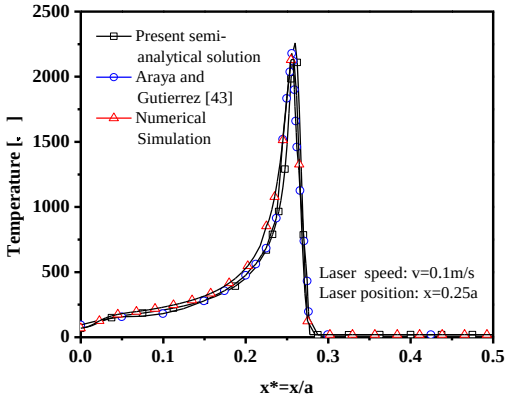

Fig.3. Comparison of the semi-analytical solution with numerical simulation and Ref.[43] along the x-direction

From the Fig.3, the current semi-analytical solution is compared with numerical solution simulated by Abaqus commercial software (also in present work) and the results of the literature [43]. The three temperature curves are approximately the same, which indicates the correctness of the semi-analytical solution and numerical solution. There is a preheat zone in front of the laser spot due to thermal conduction. The temperature gradient near the area of laser heat source is very steep, and it drops to room temperature quickly far from the laser spot. The peak temperatures of semi-analytical solution, literature, and numerical simulation are 2259 ℃, 2178℃, and 2134℃, respectively. The peak temperature of the simulation and the calculation time are closely related to the division of the grid. Hence, it is important to select the reasonable partition grid.

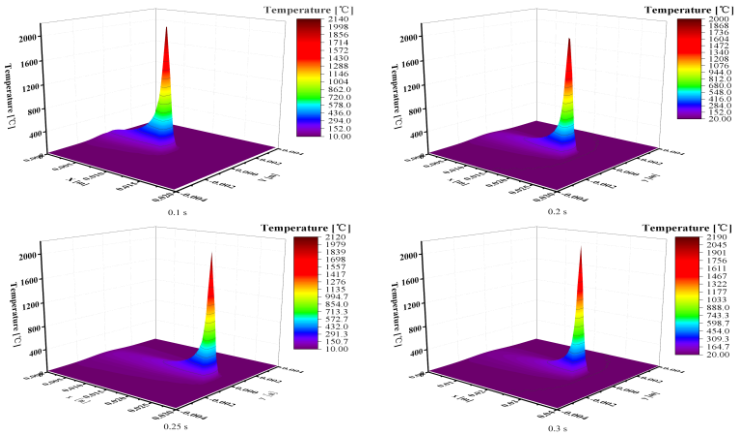

Fig.4. Three-dimensional temperature distribution on the workpiece surface at different moving distances

Example 2. Only changing the laser moving time, and the corresponding temperature distribution are obtained. Here, the x-direction grid is divided evenly, and the grids in the y and z directions are divided proportionally (the grid near the laser region is denser, and the grid farther away from the laser region is sparse).

Fig.4 shows the typical results of temperature distribution for uniform plate at various moving distances (0.1s, 0.2s, 0.25s and 0.3s location). The shape of the temperature distribution for workpiece surface is also of a Gaussian form as the Gaussian-distribution laser source is considered.

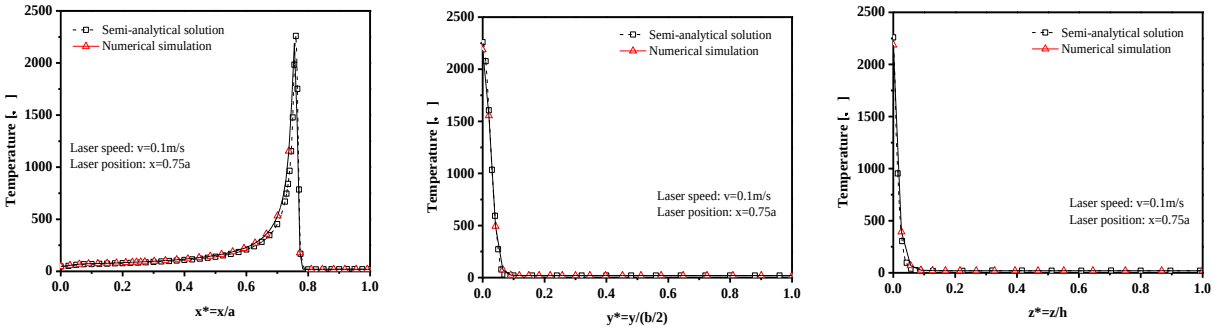

(a) (b) (c)

Fig.5. Comparison of the semi-analytical solution with numerical simulation along the x-(a), y-(b) and z-(c) directions, respectively

The comparison between the semi-analytical solution and the numerical solution simulated by Abaqus commercial software are shown in Fig.5(a)-Fig.5(c). From the Fig.5(a)-Fig.5(c), the temperature profiles of the workpiece along the x, y and z directions are well consistent when the heat source is located at $x = 0.75a$. The peak values of temperature for the semi-analytical solution and the numerical simulation are 2260℃ and 2188℃, respectively. Compared with the Fig.3, the peak temperature of the Fig.5(a) increases slightly with the increasing of the laser moving distance. Furthermore, from the Fig.5, it is noteworthy that the peak values of temperature for both curves lag behind the laser center.

Fig.5(b) and Fig.5(c) show the temperature distribution along the y ($z = 0$ surface) and z ($y = 0$ location) directions of the uniform plate, respectively. As shown in the both two figures, the farther away from the center of the spot is, the lower is the temperature. Besides, it can be found that the temperature values along the y-axis and z-axis directions reach room temperature at $0.07b/2$ and $0.06h$, respectively. That is, the temperature gradient along the y-axis decreases more moderately as well as distributed more evenly.

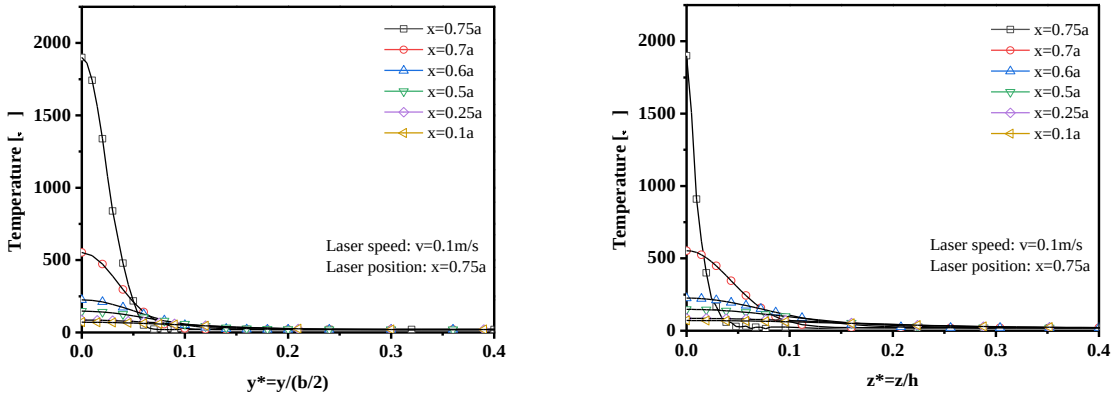

(a) (b)

Fig.6. Temperature profiles along the y-(a) and z-(b) directions, of which over and

behind the laser spot position

Fig.6(a) and Fig.6(b) show the trends of the temperature profile for the uniform plate along the y ($z=0$ surface) and z ($y=0$ location) directions, respectively, where z remains unchanged, only the different x locations is considered. From the Fig.6(a), the temperature change in the y direction is smooth at the laser center, but the change in the z direction is a little sharp from the Fig.6(b). The temperature value at the laser center drops rapidly as it can be seen from the both two figures that the temperature value at $x=0.75a$ is approximately 3.5 times than that at $x=0.7a$ location.

Example 3. This example mainly studies the effect of the heat source model on the temperature distribution for uniform plate. Herein, the size of the workpiece as well as speed of laser do not change, then the temperature distribution along the x direction of uniform plate when the laser moves to $0.25a$ ($y=0, z=0$) with different k values is considered.

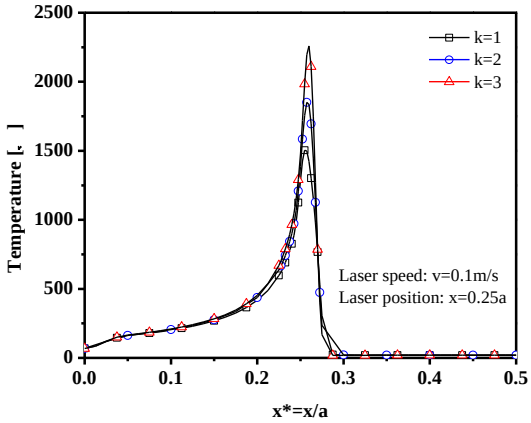

Fig.7. Effect of heat source model k on temperature distribution along the x-direction

Fig.7 shows that the larger the k-value is, the thinner and higher is the energy density distribution curve as well as the steeper for the temperature gradient near the core area of laser source. For different heat source models, the temperature distributions in the preheating zone ($x<0.2a$) and the tail zone ($x>0.3a$) are almost the same, besides the size of heat affected zone size along the x direction is also almost the same.

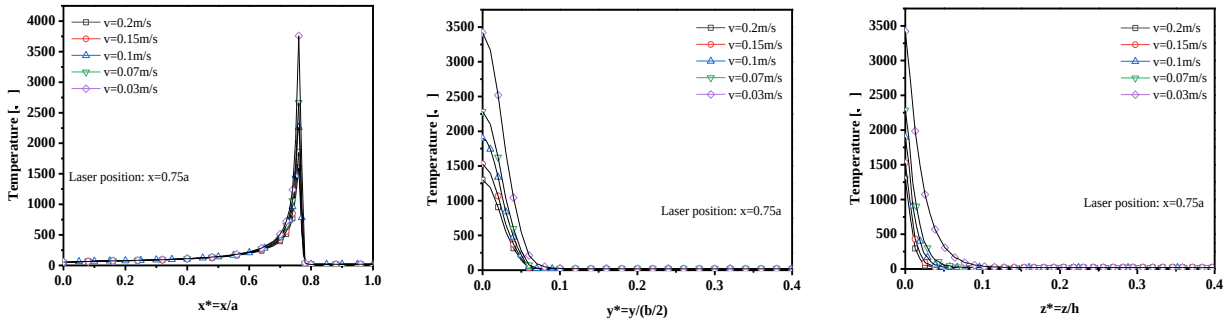

(a) (b) (c)

Fig.8. Effect of laser moving speed on temperature distribution along the x-(a), y-(b) and z-(c) directions

Example 4. Fig.8(a)-Fig.8(c) show effect of laser moving speed on temperature distribution for the uniform plate. Herein, the k value is selected as 3 and the laser source is located at $x=0.75a$ position.

The laser moving speed affects the overlap rate of spot during laser processing directly, hence increasing the laser moving speed can reduce the heat accumulation effect during the process. From the Fig.8(a), the laser moving speed cannot change the time of energy conduction, but it has a great influence on the temperature change of the material's heat affected zone, while effect on the temperature of the preheating zone on the surface of the uniform plate is too little and can be ignored.

From the Fig.8(b), the temperature gradient in the y direction decreases immediately, and the maximum surface temperature is more higher due to the limit of area for workpiece as well as continuous laser heating on the surface of plate. The farther from the center of the spot radius it is, the lower is the temperature for the uniform plate and decays in exponential form. Besides, the temperature gradient changes rapidly due to the heating effect of the laser beam on the workpiece surface is just in the laser spot radiation area, while the workpiece is only affected by thermal radiation on the non-radiation area of the laser heat source, hence the temperature gradient change at this area is slower when compared with the heated surface.

Fig.8(c) shows that the temperature as well as deposition of energy decrease with the increasing of laser moving speed at the laser source area, and the larger z becomes, the lower the temperature is. The cutting tool should be as close to the spot as possible to achieve the purpose of processing when laser-assisted processing is performed as the thickness of the affected workpiece is limited. Besides, from the Fig.8(a) to Fig.8(c), it can also be observed that the heat-affected zones in the three directions of x, y and z decrease with the increasing of laser moving speed.

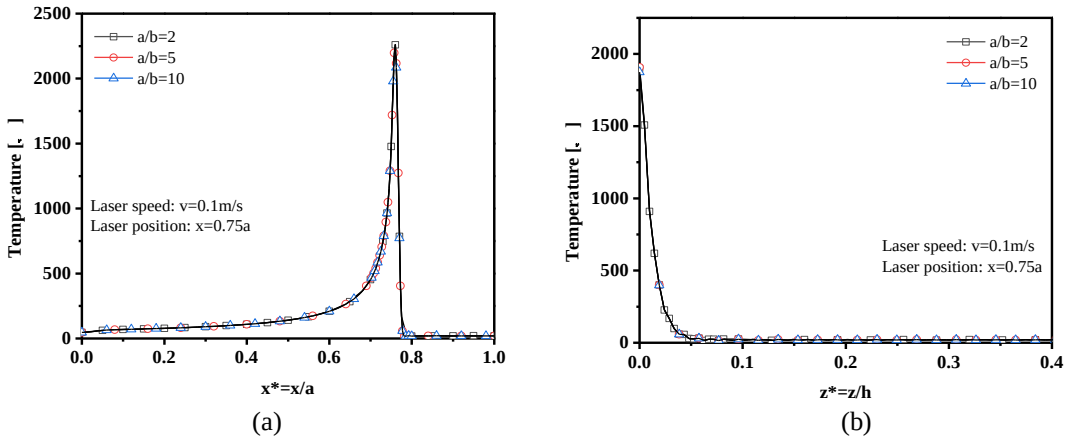

Fig.9. Effect of aspect ratio a/b on temperature distribution along the x- (a) and z-(b) directions

Example 5. The effect of different aspect ratios on the temperature distribution is studied, and the laser speed is selected as 0.1m/s in this example. The length and height of the workpiece are not changed, besides the length-width ratio 2, 5 and 10 are considered, respectively. Fig.9(a) and Fig.9(b) demonstrate effect of aspect ratio a/b on temperature distribution along the x-direction ($y=0, z=0$) and z-direction ($y=0$), respectively. With the change of the aspect ratio a/b, the temperature distribution in the area that away from the light spot does not change, and only the tiny area at the laser spot has a slight influence for the temperature. Therefore, it can be concluded that changing the size of the workpiece is not a feasible method to control the temperature distribution.

5. Conclusions

In this study, one semi-analytical solution for describing the three-dimensional transient temperature distribution caused by the moving laser heat source in the finite uniform plate is determined. The effect of

Gaussian-distribution heat source parameters k, laser moving speed and workpiece aspect ratio a/b on the temperature distribution are analyzed systematically.

The results show that the peak temperature lags behind the center of the laser and the temperature changes very steeply around the center of the laser source. The temperature in the preheating zone increases while the temperature in the tail zone remains constant essentially. The larger the k value is, the more concentrated is the energy density distribution in the laser spot as well as and the higher for the maximum temperature of the workpiece. The smaller the laser moving speed is, the more energy is deposited into the workpiece as well as the higher for the workpiece temperature. The aspect ratio of the workpiece has no significant effect on the temperature distribution, thus adjusting the temperature distribution by changing the aspect ratio of the workpiece is not feasible.

Acknowledgements

The work is supported by the National Natural Science Foundation of China (11702247, 51775510, 51875523), Zhejiang Provincial Natural Science Foundation of China (LQ17A020001) and NSF of Zhejiang University of Science and Technology (grant: F701108H08). We thank the referee and editors for the helpful comments and questions, which have improved the manuscript.

Nomenclature

a, b, h	Dimension in the x, y and z directions [m]
c	Specific heat [J/(kg℃)]
q	Heat flow absorbed by the workpiece [J]
q''	Heat flux [J/m^2]
q'''	Heat generation [J/m^2]
t	Time [s]
ΔT	Temperature increment [℃]
T	Actual temperature [℃]
T_0	Surrounding environment temperature [℃]
v	Velocity of the laser beam [m/s]
x, y, z	Cartesian coordinates [m]
α	Thermal diffusivity [m^2/s]
I_0	Intensity at the center of the spot [W/m^2]
r	Laser spot radius [m]
s	Laser spot area [m^2]

Greek

λ	workpiece thermal conductivity(W/m℃)
ρ	Density [kg/m^3]
δ	Dirac delta function

References

[1] Trdan, U., et al., Application of massive laser shock processing for improvement of mechanical and tribological properties, *Surf. Coat. Tech.*, 342 (2018), pp. 1-11

[2] Wang, H.S., et al., Application of laser remelting process on the Zr-Cu based alloy composite, *Intermetallics*, 95 (2018) pp. 11-18

[3] Zaffino, R., et al., Preparation and characterization of micro-nano engineered targets for high-power laser experiments, *Microelectron. Eng.*, 194 (2018), pp. 67-70

[4] Scisciò, M., et al., Analysis of induced stress on materials exposed to laser-plasma radiation during high-intense laser experiments, *Appl. Surf. Sci.*, 421 (2017) pp. 200-204

[5] Zhan, Y., et al., Experiment and numerical simulation for laser ultrasonic measurement of residual stress, *Ultrasonics*, 73 (2017), pp. 271-276

[6] Lax, M., Temperature rise induced by a laser beam, *J. Appl. Phys.*, 48 (1977) pp. 3919-3924.

[7] Li, J., et al., Numerical simulation and experiment of high brightness tapered lasers, *Optik*, 158 (2017), pp. 502-507

[8] Erfan, M.R., et al., Moving perforation of rocks using long pulse Nd:YAG laser, *Opt. Laser. Eng.*, 94 (2017), pp. 12-16

[9] Ragavendran, M., et al., Optimization of hybrid laser-TIG welding of 316LN steel using response surface methodology (RSM), *Opt. Laser. Eng.*, 94 (2017), pp. 27-36

[10] Wang, H., et al., A model to calculate the laser absorption property of actual surface, *Int. J. Heat Mass Tran.*, 118 (2018), pp. 562-569

[11] Zhou, Y.H., et al., Layered surface structure of gas-atomized high Nb-containing TiAl powder and its impact on laser energy absorption for selective laser melting, *Appl. Surf. Sci.*, 441 (2018), pp. 210-217

[12] Zhong, Y., et al., Effective mass dependence in laser-induced absorption of ZnO pumped by mid-infrared laser pulse, *Opt. Commun.*, 395 (2017), pp. 261-266

[13] Hu, C., et al., Enzyme-triggered size shrink and laser-enhanced NO release nanoparticles for deep tumor penetration and combination therapy, *Biomaterials*, 168 (2018), pp. 64-75

[14] Bunaziv, I., et al., Deep penetration fiber laser-arc hybrid welding of thick HSLA steel, *J. Mater. Process. Tech.*, 256 (2018), pp. 216-228

[15] Li, Y., et al., Phase evolution of ductile iron during laser cladding processing, *Surf. Coat. Tech.*, 339 (2018), pp. 37-47

[16] He, X., et al., IR laser induced phase change behaviors of the NaCl solution in the microchannel, *Chem. Eng. Sci.*, 187 (2018), pp. 318-326

[17] He, X., et al., Pulsating flow triggered by the laser induced phase change in microchannels with sawtooth-shaped baffles, Sensor. *Actuat. B-Chem.*, 260 (2018), pp. 1018-1024

[18] Vilanova-Martínez, P., et al., Laser heating induced phase changes of VO_2 crystals in air monitored by Raman spectroscopy, *J. Alloy Compd.*, 661 (2016), pp. 122-125

[19] Lei, S. and Shin, Y.C., Experimental investigation of thermo-mechanical characteristics in laser-assisted machining of silicon nitride ceramics, *J. Manuf. Sci. Eng.*, 123 (2001), pp. 639-646

[20] Rozzi, J.C., Experimental and theoretical evaluation of the laser assisted machining of silicon nitride, Ph. D. thesis, Purdue University, USA, 1997

[21] Rozzi, J.C., et al., Experimental evaluation of the laser-assisted machining of silicon nitride ceramics, *J. Manuf. Sci. Eng.*, 122 (2000), pp. 666-670

[22] Rozzi, J.C., et al., Transient, three-dimensional heat transfer model for the laser assisted machining of a silicon nitride ceramic: Part I- comparison with measured surface temperature histories, *Int. J. Heat Mass Tran.*, 43 (2000), pp. 1409-1424

[23] Rebro, P.A., et al., Laser-assisted machining of reaction sintered mullite ceramics, *J. Manuf. Sci. Eng.*, 124 (2002), pp. 875-885

[24] Mochida, Y., et al., Ultra-high-speed grinding of Si3N4 ceramics, *J. Ceram. Soc. Jpn.*, 105 (1997), pp. 784-788

[25] Li, C., et al., Simulation of the effect of spot size on temperature field and weld forming in laser tissue welding, *Optik*, 155 (2018), pp. 315-323

[26] Wu, X.X., et al., Application of ANSYS software in temperature field value simulation of laser welding, *J. Electr. Weld Mach.*, 32 (2002), pp. 1-3

[27] Gutierrez, G. and Araya, J.G., Temperature distribution in a finite solid due to a moving laser beam, ASME 2003 International Mechanical Engineering Congress and Exposition, American Society of Mechanical Engineers, Washington, DC, USA, 2003, Vol. 3, pp. 259-271

[28] Woo, H.G. and Cho, H.S., Three-dimensional temperature distribution in laser surface hardening processes, *Proc. Instn. Mech. Engrs.*, 213 (1999), pp. 695-712

[29] Han, G.M., et al., Dynamic simulation of the temperature field of stainless steel laser welding, *Mater. Design*, 28 (2007), pp. 240-245

[30] Donald, R.W. and Bathe, K.J., An efficient algorithm for analysis of nonlinear heat transfer with phase changes, *Int. J. Numer. Meth. Eng.*, 18 (1982), pp. 119-134

[31] Agarwal, P.K. and Brimacombe, J.K., Mathematical model of heat flow and austenite-pearlite transformation in eutectoid carbon steel rods for wire, *Metall. Mater. Trans. B*, 12 (1981), pp. 121-133

[32] Yao, G.F. and Chen, G.N., Numerical simulation of transient thermal field in laser melting process, *J. App. Math. Mech.*, 25 (2004), pp. 945-950

[33] Hu, Z., et al., Numerical simulation of temperature field distribution for laser sintering graphene reinforced nickel matrix nanocomposites, *J. Alloy Compd.*, 688 (2016), pp. 438-448

[34] Li, Y., et al., Modeling temperature and residual stress fields in selective laser melting, *Int. J. Mech. Sci.*, 136 (2018), pp. 24-35

[35] Elsen, M.V., et al., Solutions for modeling moving heat sources in a semi-infinite medium and applications to laser material processing, *Int. J. Heat Mass Tran.*, 50 (2007), pp. 4872-4882

[36] Cheng, P.J. and Lin, S.C., An analytical model for the temperature field in the laser forming of sheet metal, *J. Mater. Process Tech.*, 101 (2000), pp. 260-267

[37] Brockmann, R., et al., Calculation of temperature field in a thin moving sheet heated with laser beam, *Int. J. Heat Mass Tran.*, 46 (2003), pp. 717-723

[38] Jiang, H.J. and Dai, H.L., Analytical solutions for three-dimensional steady and transient heat conduction problems of a double-layer plate with a local heat source, *Int. J. Heat Mass Tran.*, 89 (2015), pp. 652-666

[39] Jiang, H.J., et al., High-energy laser shock processing for a rectangular HSLA steel plate considering solid-liquid-vapor phase change, *Appl. Therm. Eng.*, 93 (2016), pp. 384-396

[40] Jiang, H.J. and Dai, H.L., Effect of laser processing on three dimensional thermodynamic analysis for HSLA rectangular steel plates, *Int. J. Heat Mass Tran.*, 82 (2015), pp. 98-108

[41] Winczek, J., et al., Analytical description of the temperature field induced by laser heat source with any trajectory, *J. Procedia Eng.*, 149 (2016), pp. 553-558

[42] Chen W. Q., et al., General solutions for elasticity of transversely isotropic materials with thermal and other effects: A review, *J. Therm. Stresses*, 42 (2019), pp. 90-106

[43] Araya, G. and Gutierrez, G., Analytical solution for a transient, three-dimensional temperature distribution due to a moving laser beam, *Int. J. Heat Mass Tran.*, 49 (2006), pp. 4124-4131
[44] Frank, P.I., et al., *Fundamentals of heat and mass transfer*, fourth ed., New York, USA, 1996
[45] Touloukian, Y.S., et al., *Thermophysical properties of matter*, TPRL Inc. Washington, USA, 1970